2011 IEEE Nanotechnology Materials and Devices Conference
October 18-21, 2011, Jeju, Korea.

Contact improvement using E-beam and FIB deposited tungsten in carbon nanofiber interconnects

Nobuhiko Kanzaki[1], Patrick Wilhite[1], Shusaku Maeda[2], Toshishige Yamada[1], and Cary Y. Yang[1]
[1]Center for Nanostructures, Santa Clara University, Santa Clara, CA 95053, USA
[2]Hitachi High-Technologies Corporation, Ibaraki, Japan
Email: NKanzaki@scu.edu

***Abstract* −In a carbon nanofiber (CNF) interconnect device, electrode contacts formed by tungsten (W) deposition using focused ion beam is effective in reducing the contact resistance, but can potentially damage the test device because of its high energy. We present here a comparison of results for CNF interconnect devices with contacts formed by electron-beam-induced and focused-ion-beam-induced W depositions.**

Index Terms – carbon nanofiber, contact resistance, tungsten deposition, e-beam, focused ion beam

I. Introduction

As the downward scaling of integrated circuits continues, the reliability of copper interconnects due to electromigration becomes increasingly problematic. Carbon nanofiber can potential replace copper in on-chip interconnects because of its excellent thermal and electrical properties and vertically aligned growth at low temperature. To consider CNF as an on-chip interconnect material, the contact resistance between it and the metal electrode must be optimized. Using lithographic techniques to form contacts between CNF and metal electrodes requires a complicated and costly fabrication process [1]. Thus we recently proposed an alternative method using focused ion beam (FIB) [2]. The resulting total resistance decreased by a factor of about 1000 from that of the pre-W-deposited device [2]. However, FIB has the risk of damaging the on-chip devices because of its high beam energy, and gallium from the ion beam could result in device contamination. To address this problem, we have developed a technique for W deposition using a well-controlled electron beam in a variable-pressure scanning electron microscope (VP-SEM). In this technique, the source gas is delivered via a gas injection system (GIS) [3] and guided by the focused electron beam to deposit W on a selected target, with an energy significantly lower than that of FIB.

II. Sample Preparation

CNFs were grown using plasma-enhanced chemical vapor deposition (PECVD), with acetylene (C_2H_2) as the carbon source, ammonia (NH_3) as a reducing agent, and nickel (Ni) as catalyst [4]. After growth, the CNFs were suspended in isopropyl alcohol (IPA), and drop-casted between a pair of patterned gold (Au) electrodes on a SiO_2 substrate.

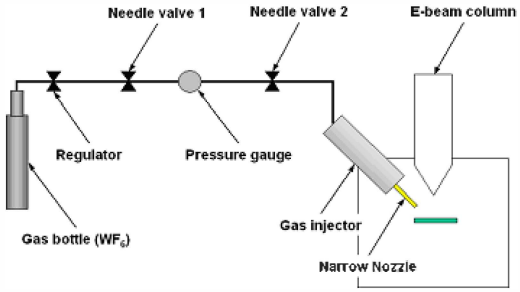

Fig. 1 Schematic of a gas injection system for e-beam deposition.

Figure 1 shows a schematic of the GIS, installed in the chamber of a VP-SEM. For electron-beam-induced deposition (EBID) of W, WF_6 is used as the source gas. WF_6 is injected onto the test device through the injector nozzle. In this study, the working distance inside the SEM chamber is set to 12.5 mm, and the distance between the device electrode and the nozzle tip is within 0.1 mm. The electron beam acceleration voltage is 30 kV and beam current is 150 μA. Tungsten contacts prepared by ion-beam induced deposition (IBID) utilized $W(CO)_6$ as the source gas in the FIB system [2].

After drop-casting the CNFs on the test chip, the devices underwent heating (~200ºC) on a hotplate in atmosphere to remove the excess IPA. Tungsten is then deposited on the CNF-Au electrode contacts using IBID and EBID. Figure 2 shows two CNF test devices after W depositions.

978-1-4577-2141-0/11/$26.00 ©2011 IEEE

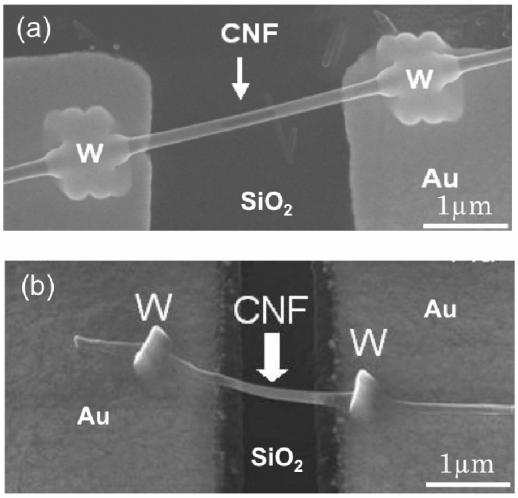

Fig. 2 SEM images of CNF test devices with deposited W on electrode contacts using (a) IBID and (b) EBID.

III. Compositions in Deposits

In EBID versus IBID comparisons, the main drawback of EBID has been lower purity in the deposits [5]. The assessment of both techniques is made difficult by the use of dissimilar source gases, and overall deposition conditions. The conditions for EBID deposition were determined from tests to enhance the W content [6]. Figure 3 shows the atomic compositions in the deposited region as determined by energy dispersive x-ray spectroscopy (EDS).

The W content of the deposit is extremely important as impurities could degrade the device performance as a result of poor interface and higher contact resistance. The e-beam deposit does not contain gallium, unlike that by FIB, which could result in unwanted p-type doping in silicon devices. Each spectrum is normalized to the signal of the background silicon, and the background spectra (taken at a similar spot without W at the CNT-Au interface) are subtracted yielding the compositions shown in Fig. 3.

Fluorine from WF_6 source gas is detected in EBID deposits and probably resides near the surface, whereas the detected Ga atoms tend to be implanted inside IBID deposits. IBID depositions also result in lower carbon contents despite the presence of carbon in the source gas $W(CO)_6$. This may be due to higher decomposition rates of the source gas using IBID, and carbon contamination in the VP-SEM chamber during EBID depositions [5].

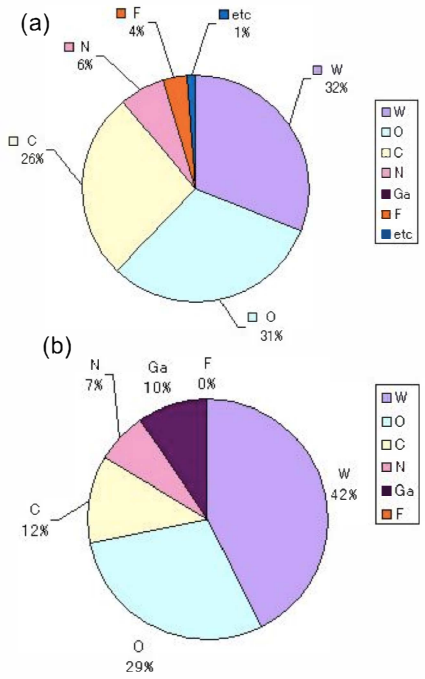

Fig. 3 EDS spectra of spots deposited by (a) EBID and (b) IBID. IBID depositions result in higher W content.

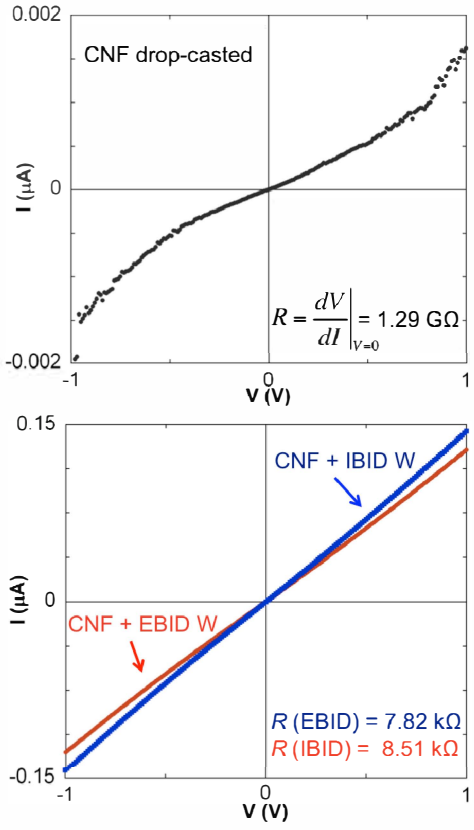

Fig. 4 I-V characteristics of CNF devices before (top plot) and after (bottom plot) W deposition. Device with EBID is indicated in red while that with IBID is in blue.

IV. I-V Characteristics

Figure 4 shows the current-voltage (I-V) characteristics of CNF devices obtained before and after W deposition. I-V characteristics of test devices with similar dimensions are comparable. While the W content in EBID deposits is generally lower than its IBID counterpart, the I-V behaviors are similar. In either case, comparing with devices prior to W deposition shown in the upper plot in Fig. 4, the total resistance drops several orders of magnitude, from GΩ to a few kΩ.

The degree of linearity in the I-V curve is a useful indication of the quality of the electrode contacts. If the CNF-electrode interface is poor, the measured I-V behavior is generally non-linear [2,7]. Both the substantial drop in resistance and the linearity in the I-V curve show that the CNF and electrode contact is significantly improved by the W deposits, using either the EBID or IBID technique [2,8].

V. Resistance Measurement

To extract the total contact resistance of CNF with W deposition, we prepare devices in a four-point-probe (4PP) test configuration and compare their resistances obtained using two-point-probe (2PP) and 4PP measurements. Figure 5(a) shows the SEM images of such a device with EBID W. The measured resistances are 4.39 kΩ and 3.90 kΩ using 2PP and 4PP measurements, respectively. Thus the total contact resistance is 0.49 kΩ, substantially improved by W deposition.

Using the results from 4PP measurements, we can also extract the resistivity of the CNF. For the device in Fig. 5, with diameter 219nm and length 3.85μm, and the extracted resistivity is 3.83×10^{-3}Ωcm. This value is similar 4.2×10^{-3}Ωcm for CNFs with Au/Ti contacts formed by e-beam lithography [1].

To investigate the resistance behavior of CNFs under current stressing, we prepare several devices in a 2PP test configuration with IBID and EBID W (such as those in Fig. 2) and apply progressively increasing stress current with an increment of 50μA till breakdown and measure the resistance after each stress cycle.

Figure 6 shows the measured resistance behavior of the CNF devices as a function of stress current. The resistance of each device with different diameter and length remains fairly constant until breakdown occurs, for either the IBID or EBID case.

We convert stress current to temperature using our heat transport model [9]. The contact resistance is ignored in this analysis. Figure 7 reveals the Arrhenius behavior of the EBID W CNF devices. This result confirms our previous findings for CNFs in both vertical and horizontal configurations that the CNF conductivity is of activation-type in nature [2,10,11]. It further supports our previous suggestion that, this temperature dependence is due to carrier trapping and detrapping at defect sites within the carbon nanostructure.

From the gradient values in Fig. 7, we extract the activation energy ΔE in $\sigma(T) = \sigma_0\exp(-\Delta E/k_BT)$. ΔE = 30 meV for IBID W and 15 meV for EBID W. This difference in activation energy is currently under investigation.

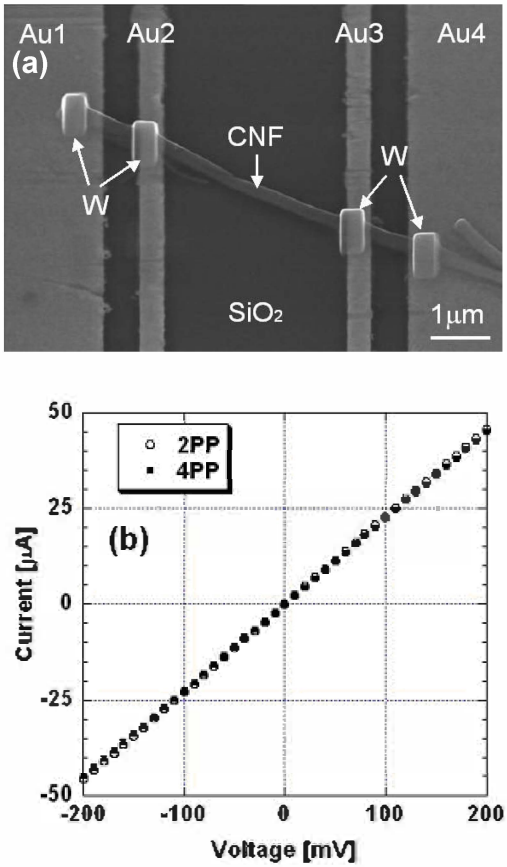

Fig. 5 (a) SEM images of 4PP test device with EBID-W contacts and (b) I-V characteristics of 2PP and 4PP measurements.

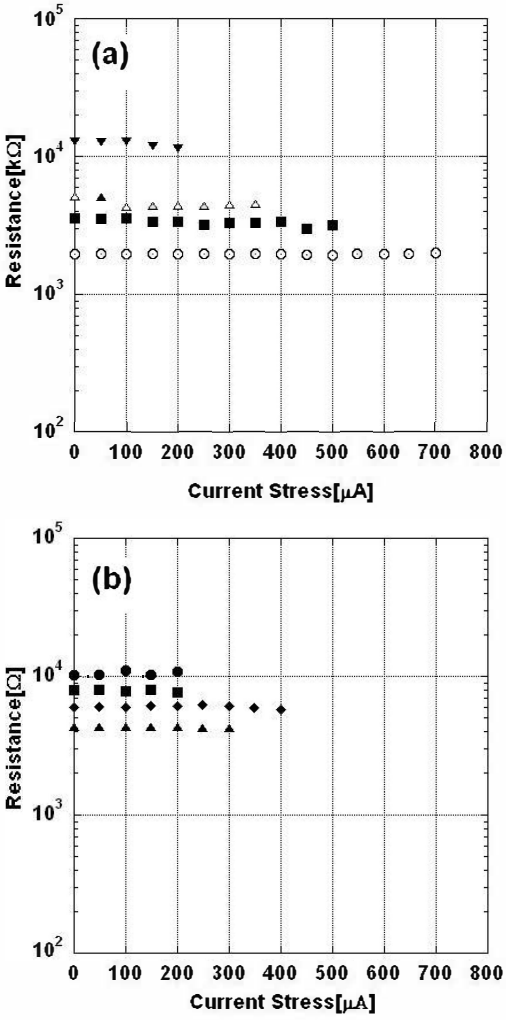

Fig. 6 Resistance of CNF devices with (a) IBID-W and (b) EBID-W deposition as a function of current stress, measured after each stress cycle.

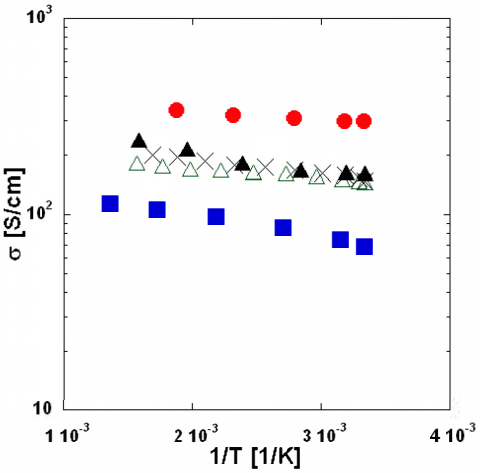

Fig. 7 Conductivity of five EBID-W CNF devices as a function of inverse temperature.

VI. Conclusion

We have shown that W depositions formed on CNF-Au electrodes result in low-resistance contacts for CNF interconnect test devices. Despite the smaller W content in EBID deposits, the measured resistance and I-V behavior are comparable to their counterparts for IBID W devices [2], as well as those with Au/Ti contacts fabricated using e-beam lithography. We have also confirmed using current stressing measurements the Arrhenius behavior of the CNF conductivity for devices with either EBID or IBID-W contacts.

Acknowledgments

The authors acknowledge the technical support from Hitachi High Technologies America, and the expert advice from Philip D. Rack and David C. Joy of the University of Tennessee on the gas injection system. This work was supported by the United States Army Space and Missile Defense Command (SMDC) and carries Distribution Statement A, approved for public release, distribution unlimited.

References

[1] L. Zhang, D. Austin, V. I. Merkulov, A. V. Meleshko, K. L. Klein, M. A. Guillorn, D. H. Lowndes and M. L. Simpson, Appl. Phys. Lett. **84**, 3972 (2004).

[2] T. Saito, T. Yamada, D. Fabris, H. Kitsuki, P.Wilhite, M. Suzuki, and C.Y. Yang, Appl. Phys. Lett. **93**, 102108 (2008).

[3] D.C. Joy and P. D. Rack, Microscopy and Microanalysis, NY, **11**, 816 (2005).

[4] B. A. Cruden, A. M. Cassell, Q. Ye, and M. Meyyappan, J. Appl. Phys. **94**, 4070 (2003).

[5] A. Botman, J. J. L. Mulders and C. W. Hagen, Nanotechnology **20**, 372001 (2009).

[6] K. L. Klein, S. J. Randolph, J. D. Fowlkes, L. F. Allard, H. M. Meyer, M. L. Simpson, P. D. Rack, Nanotechnology **19,** 345705 (2008).

[7] T. Yamada, T. Saito, M. Suzuki, P. Wilhite, X. Sun, N. Akhavantafti, D. Fabris, and C. Y. Yang, J. Appl. Phys. **107**, 044304 (2010).

[8] S. Maeda, P. Wilhite, N. Kanzaki, T. Yamada and C.Y. Yang, AIP Advances **1**, 022102 (2011).

[9] T. Yamada, T. Saito, D. Fabris, and C. Y. Yang, IEEE Elect. Dev. Lett., **30** (2009).

[10]Q. Ngo, T. Yamada, M. Suzuki, Y. Ominami, A. M. Cassell, J. Li, M. Meyyappan, and C. Y. Yang, IEEE Trans. Nanotechnol., **6**, 688 (2007).

[11] T. Yamada, H. Yabutani, T. Saito and C. Y. Yang, Nanotechnology, **21**, 26707 (2010).